

# Molecular Dynamics Simulations of the Bacterial ABC Transporter SAV1866 in the Closed Form

Jean-François St-Pierre,<sup>†</sup> Alex Bunker,<sup>‡,||</sup> Tomasz Róg,<sup>§</sup> Mikko Karttunen,<sup>¶</sup> and Normand Mousseau<sup>\*,†</sup>

<sup>†</sup>Département de Physique and Regroupement Québécois sur les Matériaux de Pointe, Université de Montréal, C.P. 6128, succursale centre-ville, Montréal (Québec), Canada H3C 3J7

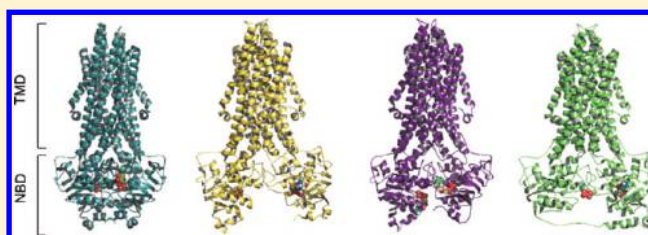
<sup>‡</sup>Centre for Drug Research, Faculty of Pharmacy, University of Helsinki, PO Box 56, FI-00014 University of Helsinki, Finland

<sup>§</sup>Department of Physics, Tampere University of Technology, PO Box 692, FI-33101 Tampere, Finland

<sup>¶</sup>Department of Chemistry, University of Waterloo, 200 University Avenue West, Waterloo, Ontario, Canada N2L 3G1

<sup>||</sup>Department of Chemistry, Aalto University, PO Box 6100, FI-02015 Aalto, Finland

**ABSTRACT:** The ATP binding cassette (ABC) transporter family of proteins contains members involved in ATP-mediated import or export of ligands at the cell membrane. For the case of exporters, the translocation mechanism involves a large-scale conformational change that involves a clothespin-like motion from an inward-facing open state, able to bind ligands and adenosine triphosphate (ATP), to an outward-facing closed state. Our work focuses on SAV1866, a bacterial member of the ABC transporter family for which the structure is known for the closed state. To evaluate the ability of this protein to undergo conformational changes at physiological temperature, we first performed conventional molecular dynamics (MD) on the cocrystallized adenosine diphosphate (ADP)-bound structure and on a nucleotide-free structure. With this assessment of SAV1866's stability, conformational changes were induced by steered molecular dynamics (SMD), in which the nucleotide binding domains (NBD) were pushed apart, simulating the ATP hydrolysis energy expenditure. We found that the transmembrane domain is not easily perturbed by large-scale motions of the NBDs.



## INTRODUCTION

ABC transporters are a family of over 1000 proteins involved in active, i.e., nondiffusive, ATP-hydrolysis-dependent transport of ligands across cell membranes.<sup>1–4</sup> They transport vital molecules such as lipids, steroids, and vitamins<sup>2</sup> and, as a result, are involved in drug transport.<sup>5</sup> Mutations that affect the expression of ABC transporters can have severe consequences. Overexpression of ABC transporters is the leading cause of chemotherapy resistance in cancer treatment.<sup>6</sup>

ABC transporters belong to the class of membrane-spanning proteins. It is well-known that the structural characterization of membrane proteins is particularly difficult (see, for example, ref 7) and hence it has not been easy to obtain full crystal structures. The structures of individual domains have, however, enabled computational modeling studies, which have provided significant insight into the structure–function mechanisms of ABC transporters.<sup>8–16</sup>

Structurally, all ABC transporters, whether eukaryotic or not, have two pairs of domains: the transmembrane domains (TMD) and the nucleotide binding domains (NBD). The former may have considerable sequence variations, but the latter are highly conserved.<sup>2</sup> Since full ABC transporters display a structural radial symmetry, they have two TMD and two NBD domains which can be encoded by an individual gene for each domain, by a gene containing one TMD and one NBD, or

by a gene containing the full TMD–NBD–TMD–NBD sequence.

The NBDs hydrolyze two ATP molecules to provide the energy necessary for the efflux cycle. Both domain pairs are believed to move toward each other during the transport cycle, as the protein undergoes a transition from the open, ligand binding, to the closed, ligand expelling, conformation. Figure 1 shows crystal structures of two ABC transporters, mouse P-glycoprotein (permeability glycoprotein)<sup>17</sup> in the open conformation and its close bacterial homologue SAV1866<sup>18</sup> in the closed conformation. The figure shows that the conformational change the protein undergoes during the efflux cycle involves both a large (~2 nm) displacement of the NBDs and the transformation from an open conformation with an inward facing cavity exposing the allocrite binding region in the TMDs to the cytosol and the membrane's inner leaflet to a closed conformation with an outward facing cavity in the TMDs when effluxing the allocrite. Another protein of interest is MsbA for which three structures of lower resolution were obtained: an inward-facing open conformation and an outward facing closed conformation that are respectively similar to the

**Received:** September 21, 2011

**Revised:** February 14, 2012

**Published:** February 16, 2012

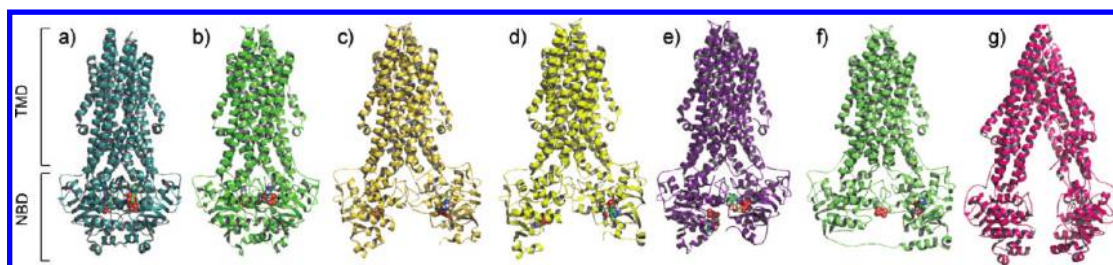


**Figure 1.** Reference crystal structures: (a) SAV1866 in closed conformation (pdb 2HYD) and (g) mouse P-glycoprotein (pdb 3GSU) in the open conformation. Final results for a range of ADP-bound simulations: (b) MD-ADP, (c) SMD-ADP1, (d) CMD-ADP1, (e) MD-ADP-RF, and (f) SMD-ADP-H204A2 (see Table 1 for details of the notation). ADP is shown in sphere representation.

P-glycoprotein and SAV1866 protein conformations mentioned above, but also a third conformation with closed NBD and inward-facing cavity.<sup>19</sup>

In the current report, we are specifically interested in the *Staphylococcus aureus* multidrug transporter SAV1866. The ability of SAV1866 to efflux a large number of drugs makes it a good general model for multidrug ABC transporters, including human P-glycoprotein,<sup>20</sup> which is involved in the transport of, for example, peptides, lipids, and various xenobiotics. SAV1866 has a homodimer structure: the sequence of each component of the dimer contains one TMD and one NBD, with the two components of the dimer symmetrically oriented along a rotation axis perpendicular to the lipid bilayer. Aittoniemi et al.<sup>15</sup> performed simulations on SAV1866 to evaluate the effect of replacing the cocrystallized ADP by the active ligand ATP and  $Mg^{2+}$  in the NBDs. They found an asymmetric reorientation of the NBD interface regions toward the TMD interface. Becker et al.<sup>13</sup> saw increased constriction of the TMD helices in the membrane in the apo structure relative to the structure with ATP bound. Oliveira et al. found,<sup>21</sup> by inserting the products of ATP hydrolysis, ADP +  $Mg^{2+}$  and inorganic phosphate (IP), evidence of TMD separation close to the NBD interface in both the substrate-bound and product-bound structures. In the most recent simulation of truncated SAV1866 with single ATP +  $Mg^{2+}$ , Jones and George<sup>22</sup> observed a rotation in the NBDs of the SAV1866 homodimer in agreement with experimental results on heterodimer NBD domains of other ABC transporters, notably of P-glycoprotein.<sup>23–25</sup> This indicates that the otherwise symmetric NBDs of SAV1866 may also undergo asymmetric transformations during the efflux cycle.

We present atomistic simulations performed on the closed form of *S. aureus* ABC transporter SAV1866 in which we investigated the large-scale structural motions that this protein may sample. We have completed two 100 ns MD simulations of the SAV1866 closed complex inserted in a dilinoleoylphosphatidylcholine (DLPC) and dilinoleoylphosphatidylethanolamine (DLPE) lipid bilayer, one in the presence of the cocrystallized ADP molecule and one with the ligand removed based on the hypothesis that these structures would favor conformation changes. We also investigated conformational changes when separating the two NBD using 20 ns SMD simulation runs. In the targeted MD performed by Weng et al.<sup>16</sup> on MsbA, all  $\alpha$ -carbons ( $Ca$ ) were forced to change conformation. We chose a different approach in our SMD simulations: A single harmonic potential between the centers of mass of the two NBDs is introduced in order to induce a transformation from the closed to the open conformation. Finally, we consider mutagenesis to test mechanisms for enhancing flexibility.

## METHODS

MD simulations were performed using the Gromacs 4 software package<sup>26</sup> with the Optimized Potentials for Liquid Simulations (OPLS-AA) all-atom force field<sup>27</sup> and periodic boundary conditions. Electrostatic interactions were computed using the particle-mesh Ewald method (PME)<sup>28,29</sup> with a real space cutoff of 1.0 nm; It was also ensured that charge groups were small, in order to avoid possible physical artifacts that have been reported in similar simulation geometries of nanotubes.<sup>30</sup> It has been shown that this choice is devoid of artifacts and leads to physically correct behavior, both static and dynamic.<sup>31,32</sup> The Lennard-Jones interactions were also cut off at 1.0 nm. SAV1866 crystal (pdb 2HYD<sup>18</sup>) was inserted in a pre-equilibrated DLPC<sup>33,34</sup>/DLPE lipid membrane of size  $16.3 \times 16.3$  nm. A hole was created in the lipid membrane through the removal of all lipids that came into contact with the membrane-aligned protein.<sup>11,35</sup> The remaining lipid membrane was composed of 217 DLPC and 175 DLPE lipids. The protein's termini were in their zwitterionic form: the histidines 103, 457, and 559 of each dimer were protonated on the  $N\delta$  atom and all other histidines were protonated on the  $N\epsilon$  atom. All aspartic acid, arginine, glutamic acid, and lysine were used in their default physiological protonation states. Protein and membrane were solvated in a water box of 17 nm in height using the TIP3P water model.<sup>36</sup>  $K^+$  and  $Cl^-$  ions were added to obtain a 140 mM concentration of KCl in order to model the cytosol while keeping the net charge of the system neutral. The simulation contained a total of  $\sim 235\,000$  atoms. The protein's backbone coordinates were harmonically restrained for a short MD simulation of 425 ps at 310 K in which the gap between the membrane and protein disappeared. Any water molecule still present at the membrane/protein interface was manually removed.

Following a 1000-step steepest descent system minimization, a 2 ns MD relaxation with a smaller integration time step of 1 fs was executed in which the temperature was increased from 10 to 310 K leading to a thermally equilibrated structure with a 0.28 nm backbone root-mean-square deviation (rmsd) from the crystal structure. The size of the final periodic box after releasing the restraints was 11.6 nm  $\times$  11.6 nm  $\times$  17.7 nm. This ensures that the protein is always at least 4 nm away from its periodic images while it is aligned perpendicularly to the membrane plane. Production runs were executed using a 2 fs time step with covalent bond length constrained by LINCS.<sup>37</sup> A snapshot of the system's conformation was saved every 20 ps for analysis purposes.

All simulations were performed twice: once with the cocrystallized ADP molecules and once on a nucleotide-free apoprotein (APO) structure. The APO conformation was

generated by removing ADP from the ADP-bound system after 20 ns of simulation time followed by a 5 ps MD simulation with restrained protein backbone atoms and 60 ps of unrestrained MD at temperatures increasing from 10 to 310 K to allow for equilibration of the water molecules in the ATP binding cavities. Initial conventional 100 ns MD simulations were completed using Berendsen weak coupling thermal and pressure bath fixed at 310 K and 1 bar with coupling time constants of 0.1 and 1.0 ps, respectively.<sup>38</sup> System conformations were saved every 20 ps for analysis.

SMD simulations were completed by pushing the centers of mass of the two NBDs apart using a harmonic potential between the centers of mass (COM) of the two NBDs at rate of 0.1 nm/ns. The force constant was set to 2.5 MJ/(mol·nm<sup>2</sup>). External forces were applied to 45 backbone atoms of residues ILE417-GLN421, ILE498-ALA504, and THR528-ALA533 from three strands of the parallel  $\beta$ -sheet found at the centers of each of the NBDs. The reasons for restraining these atoms are multiple. By applying the steering forces to a limited number of atoms with a COM located near the NBD's COM, we limit the possibility of generating unlikely structural deformations of the NBDs that artificially increasing the NBD's COM distances. The  $\beta$ -sheet structure of the selected atoms and its position at the center of the two halves of each NBD add to its structural stability. Also, the central position of the  $\beta$ -sheet's COM is less likely to induce bias in the separation angles observed when the NBDs break contact. Temperature and pressure were maintained through the Nosé–Hoover thermostat<sup>39,40</sup> and a Parrinello–Rahman barostat,<sup>41</sup> respectively, with the same coupling constants as used in the MD simulations. The work exerted by the harmonic force can be extracted through numerical integration of the force applied by the potential over time, multiplied by the total displacement.

For constant-restraint molecular dynamics (CMD), we used the same parameters as SMD, but with a null pull rate; i.e., we maintained a fixed harmonic bond length attached to the centers of mass of the two NBDs. Details concerning each method and starting conformation for all simulations are listed in Table 1. PyMol (<http://www.pymol.org/>) was used for visualization.

## RESULTS AND DISCUSSION

**MD Simulations.** The rmsd as measured from the crystalline structure is shown for both the ADP-bound and the APO proteins in Figure 2a. After a rapid growth in the first 2 ns of equilibration prior to the production runs to a rmsd of  $0.28 \pm 0.01$  nm, the rmsd slowly increases to an average of  $0.38 \pm 0.01$  and  $0.36 \pm 0.01$  nm, respectively, during the last 20 ns of each 100 ns simulation. This is in line with the average of 0.34 nm, observed by Aittoniemi et al.<sup>15</sup> with ATP and Mg<sup>2+</sup> present. While rmsd to the crystal structure of SAV1866 increases by only 0.8–1.0 nm during the production runs after equilibration, the protein is seen to explore a conformation subspace leading to rmsd values of 0.20 and 0.18 nm from the start of the production runs for MD-ADP and MD-APO, respectively. Rmsd on the pairs of TMDs and NBDs (Table 2) were also comparable to the previously published results, and slightly lower than the apoprotein simulations of Becker et al.<sup>13</sup> (Figure 2 in ref 13) and the ATP-bound and ADP-IP bound simulations of Oliveira et al. (Figure 2 in ref 21).

Looking at the rms fluctuations for each of the atoms that correlate with the diffraction B factors,<sup>18</sup> we find, as expected, that the side chains in the ATP binding cavity of the APO

**Table 1. Reference Table of All Simulations Performed in This Work, the Method Used, and Their Starting Structures<sup>a</sup>**

simulation name	initial structure	method	length (ns)
MD-ADP	crystal structure with ADP bound, inserted into membrane	MD	100
MD-APO	crystal structure inserted into membrane, ADP removed	MD	100
SMD-ADP1	MD-ADP 100 ns structure	SMD	20
SMD-ADP2	MD-ADP 100 ns structure	SMD	20
SMD-ADP-ML	MD-ADP 100 ns structure without membrane	SMD	20
SMD-ADP-H204A1	MD-ADP 100 ns structure with residues His204 mutated to Ala	SMD	20
SMD-ADP-H204A2	MD-ADP 100 ns structure with residues His204 mutated to Ala	SMD	20
SMD-APO1	MD-APO 100 ns structure	SMD	20
SMD-APO2	MD-APO 100 ns structure	SMD	20
SMD-APO-ML	MD-APO 100 ns structure without membrane	SMD	20
CMD-ADP1	SMD-ADP1 20 ns structure	CMD	14
CMD-ADP2	SMD-ADP2 20 ns structure	CMD	14
CMD-APO1	SMD-APO1 20 ns structure	CMD	14
MD-ADP-RF	CMD-ADP1 14 ns structure	MD	60
MD-APO-RF	CMD-APO1 14 ns structure	MD	60

<sup>a</sup>MD, SMD, and CMD stand for molecular dynamics, steered MD, and constant-restraint MD, and ML stands for membrane-less and RF for refolding.

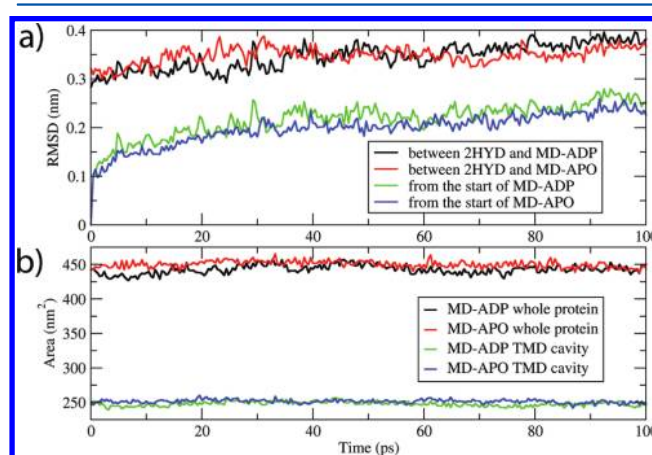


**Figure 2.** (a) Evolution of the backbone rmsd as measured from the SAV1866 crystal structure over the whole 100 ns MD trajectory for the ADP-bound (MD-ADP) and APO (MD-APO) SAV1866. Also presented is the evolution of the rmsd as measured from the start of the production simulations for MD-ADP and MD-APO. (b) Solvent-accessible surface area (SASA) of the whole protein excluding membrane contacts for MD-ADP and MD-APO and SASA of the TMD inner cavity helices calculated on residues PHE17-SER89, ASN126-GLN200, and ALA250-SER307 of each TMD.

structure show higher flexibility than the ADP-bound protein. However, there were no signs of large instabilities (data not shown). The most notable conformational changes occurred in the TMD region. In both the ADP bound and APO simulations, the TMD becomes constricted (see Figure 3). This brings helix H1 into contact with facing helices H9 and H12 and also helices H3 and H6 into contact with H7. Opposites H6 and H12 (in gray) also come into contact. When examining the number of water molecules within 0.7 nm of helices H6 and H12 throughout the MD simulations, we see a

**Table 2. Average  $\text{C}\alpha$ -Rmsd Measured over Different Domains between the Reference Initial Conformation and the Structures from Last 20 ns of MD Simulation for the ADP-Bound (MD-ADP) and APO (MD-APO) SAV1866<sup>a</sup>**

domain	ADP-bound (nm)	APO (nm)
TMD1	0.40	0.33
NBD1	0.17	0.20
TMD2	0.42	0.39
NBD2	0.19	0.19
both TMD	0.42	0.38
both NBD	0.22	0.24

<sup>a</sup>Standard deviation for all points is 0.01 nm.

diminution of 50 water molecules for MD-ADP and 20 for MD-APO between the beginning of the simulation and at time 100 ns. This reduction is not correlated by a reduction of the solvent-accessible surface area of the protein or of the cavity (Figure 2b). Similar constriction was also observed by Becker et al.<sup>13</sup> in their APO structure simulation of SAV1866 over a 80 ns MD, but not in the ATP/Mg<sup>2+</sup>-bound structure.

The lipid density plots were obtained by counting the number of lipid head groups in a region 4.5 nm away from the center of mass of the membrane-inserted protein's amino acid, divided by the corresponding periodic box's surface area minus the occlusion disk of 4.5 nm radius that contains the inserted protein's TMDs. Figure 4 shows that the TMD constriction is not caused by a pressure imbalance between the outer and inner lipid bilayer leaflets: we see no correlation between the closing motion of the TMD over the 100 ns simulation and the ratio of inner and outer leaflet lipid densities. On average, the outer leaflet lipid densities were 1.96 and 1.94 lipids/nm<sup>2</sup> for the ADP-bound and APO simulations, respectively, while they are 1.87 and 1.93 lipids/nm<sup>2</sup>, respectively, in the inner leaflet. We also noticed the standard deviation in lipid density to be 22% higher in the ADP-bound simulations than in the APO simulations.

The core helices H6 and H12 are the most deformed ones through the constriction in the bilayer zone, see Figure 5. In the ADP-bound simulation, this deformation also involves a shortening of 0.36 nm of H12 and elongation of 0.17 nm of H6 calculated as the distance between residues GLY276 and ASP319 of each helix.

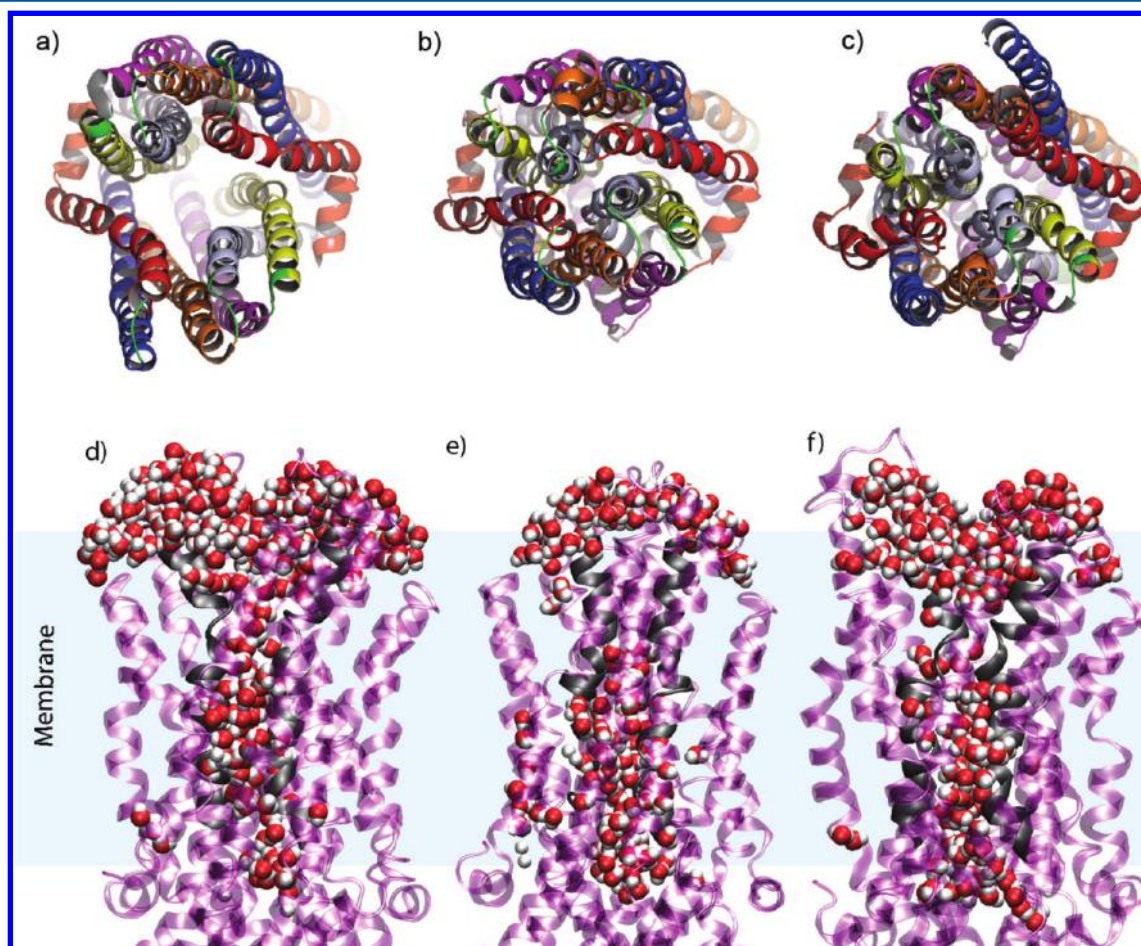


**Figure 3.** Transmembrane domain (TMD) helices viewed from the external side of the lipid membrane where (a) is the initial SAV1866 structure (pdb 2HYD), (b) is the result of 100 ns of MD for the ADP-bound structure (MD-ADP), and (c) is the result of 100 ns for the APO structure (MD-APO). Color code for the first domain helices is H1 (red), H2 (blue), H3 (yellow), H4 (magenta), H5 (orange), H6 (gray). Helices H1 through H6 of the second homodimer TMD are labeled by the same color code, respectively, and are referenced in the text by the names H7 to H12 for clarity. Also presented, cross-membrane view (d) of the starting conformation of MD-ADP, and the 100 ns conformation (e) of MD-ADP and (f) MD-APO with the residues VAL277 to PHE303 of the H6 and H12 helices in gray and all the water molecules within 0.7 nm of these residues in van der Waals representation.

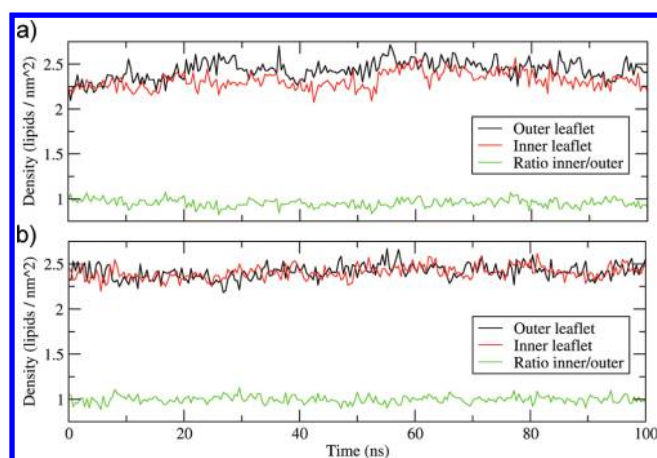


**Figure 4.** Lipid density of the bilayer leaflets of (a) ADP-bound MD simulation (MD-ADP), and (b) the APO MD simulation (MD-APO).

Helices H3–H4 and H9–H10, shown in Figure 6 and forming the core region of the lower TMD, are unaffected in the lower half but bend sharply at residue GLY183 of H4 to accommodate the constriction in a hingelike motion at the stated residue.

The amino acid interactions at the NBDs interfaces differ from those observed by Aittoniemi et al.<sup>15</sup> To compare our NBD interactions with theirs, we defined a contact ratio metric between two amino acids as the number of conformations where any atoms of an amino acid of the first dimer's NBD (NBD1) is found at a distance of less than 0.3 nm from any atoms from an amino acid of second dimer's (NBD2), divided by the total number of saved conformation snapshots.

In the following NBD analysis, when a contact between two amino acids is stated, the first amino acid is in NBD1 and the second in NBD2. Therefore, if amino acid ARG474 from NBD1 is at a distance lower than 0.3 nm from ARG474 of NBD2 in 50 conformations out of 100, then we would say that the ARG474-ARG474 contact ratio is 0.50. In both our MD simulations, we see a reorientation of both ARG474 in the membrane plane (both amino acids remain parallel to the membrane plane) but, unlike Aittoniemi et al.,<sup>15</sup> we observed no stacking. The X-ray structure contact ARG474-ARG474 is also weak in our simulations with a contact ratio of no more than 0.11 in both MD simulations. The reorientation of the

ARG474-ARG474 pair also involves a break in contact between GLN208 of TMD1 and ARG474 of NBD1 in both MD-ADP and MD-APO simulations, while the symmetrical contact is maintained between TMD2 and NBD2. Another contact of the NBDs with the TMDs which is observed to break is between TYR112 of TMD2 and GLY472 of NBD1 with a conserved symmetrical contact between TMD1 and NBD2. Aittoniemi et al. reported that ASP423-ARG474 and ARG474-ASP423 broke contact in their simulations prior to the formation of contacts ASP423-LYS483 and LYS483-ASP423, which freed ARG474 to adopt a stacked conformation along the axis perpendicular to the membrane. In our case, ASP423-ARG474 has a conserved contact ratio of 0.99 in MD-ADP and 0.20 in MD-APO, while the symmetrical ARG474-ASP423 has a contact ratio of 0.98 and 0.99, respectively. This does not prevent the formation of contact ASP423-LYS483 with contact ratio of ratio of 0.99 in MD-ADP and 0.89 in MD-APO, but it does prevent the formation of the symmetrical LYS483-ASP423 which was not found in either simulation. The later was replaced by a contact between LYS483-GLN422 with contact ratio of 0.83 in MD-ADP and 0.56 in MD-APO. This was made possible by the absence of  $Mg^{2+}$  in our simulations.  $Mg^{2+}$  interacts typically with GLN422.

In spite of these observations, we noticed only very small differences in the ADP-bound and APO NBD stability after simulations of 100 ns. To identify the opening modes on computationally accessible time scales, it is necessary to use more forceful methods such as SMD.

**Steered Molecular Dynamics.** We can simulate the injection of energy into the NBDs by exerting pressure on a group of atoms located at the center of each NBD. This is done through a harmonic potential of increasing equilibrium length connecting the various domains. For both ADP-bound and APO structures, we performed three 20 ns SMD simulations to separate the NBDs by 2 nm. In two of the cases, we replaced the lipid bilayer by water and ions to test the impact of the presence/absence of a membrane (see Table 1).

We observed two modes of NBD separation (Figure 7). The selection of a mode depended on the time it took to break the contacts between the two domains. As shown in Figure 8, the angle between the NBDs increases significantly in the plane parallel to the membrane before the 12th nanosecond in all simulations. This indicates a peeling separation where one side

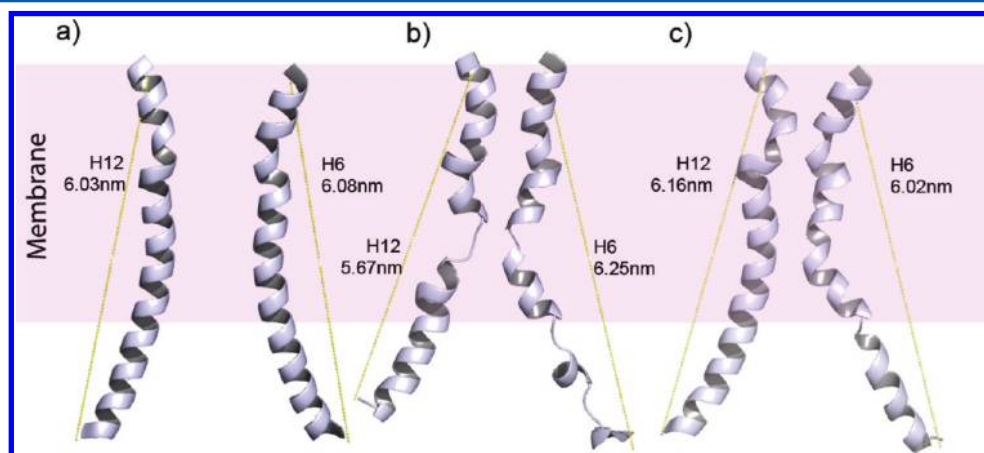


**Figure 5.** TMD helices H6 and H12 where (a) is the initial SAV1866 structure, (b) is the result of 100 ns of MD for the ADP-bound structure, and (c) is the same result for the APO structure.

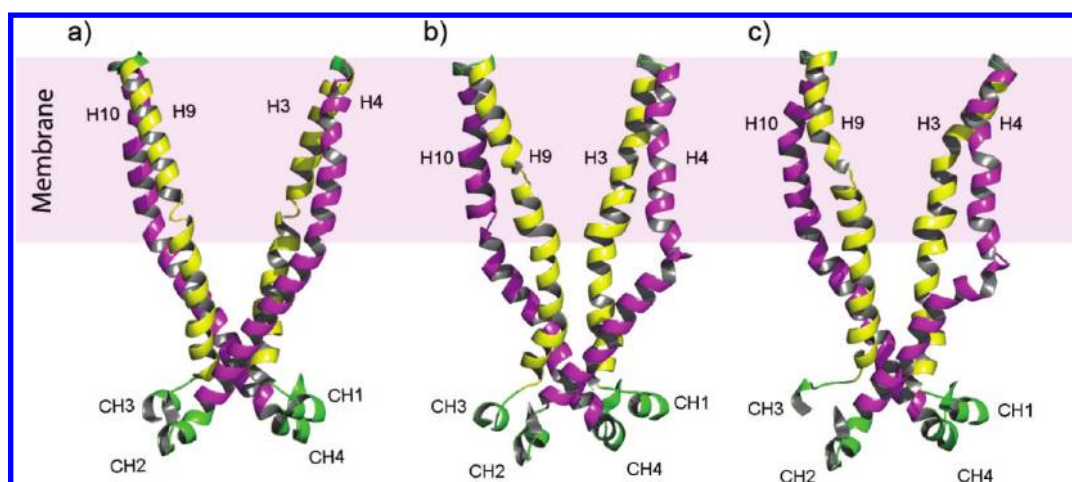


**Figure 6.** TMD helices H3–H4 and H9–H10 where (a) is the initial SAV1866 structure, (b) is the result of 100 ns of MD for the ADP-bound structure, and (c) is the same result for the APO structure.

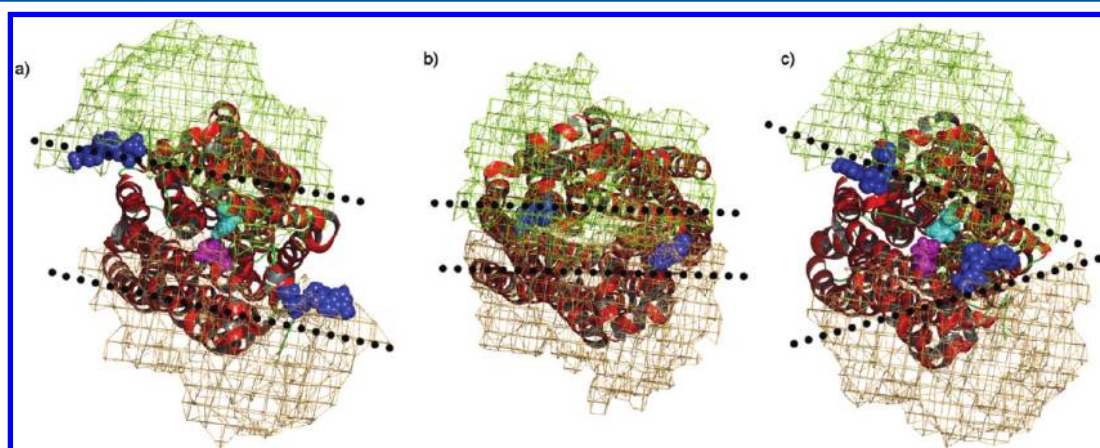


**Figure 7.** View of the nucleotide binding domains (orange and green mesh) from a position perpendicular to the cytosolic side of the membrane after 20 ns of SMD for simulations for a parallel and a skewed NBD conformation, respectively: simulations (a) SMD-ADP1 and (c) SMD-ADP2 after 20 ns with ADP in dark blue and His204 of helix H4 (cyan) and H10 (magenta). Initial structure is presented in (b). Dashed lines represent the approximate NBD–NBD surface interfaces.

of the contact interface between the two NBDs breaks before the other. In most cases, the angle between the domains converges back to parallel when the external force is released. In

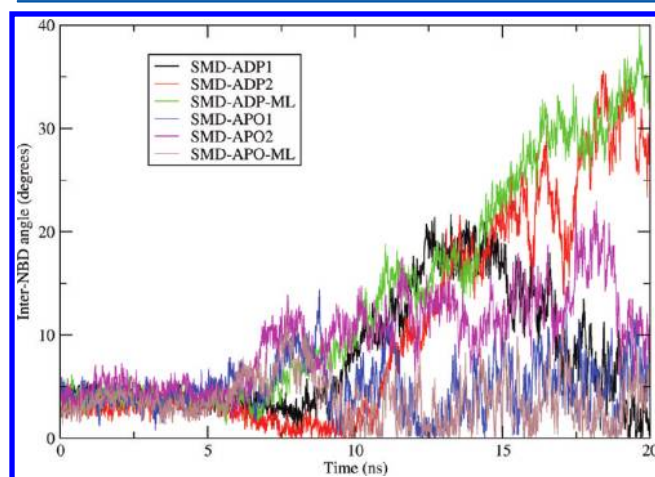


**Figure 8.** Evolution of the angle between the contact planes of the two nucleotide binding domains as a function of the SMD simulation time.

two of the cases, SMD-ADP2 and SMD-ADP-ML, the contact was maintained throughout the simulations and the angle remained at  $28^\circ$  and  $35 \pm 2^\circ$ , respectively.

In the six SMD simulations, we computed the work of opening SAV1866 by taking the integral of the force distribution on the harmonic forcing separation. Generally, we see that the presence of ADP and the presence of a lipid membrane have strong cumulative stabilizing effects (Table 3).

**Table 3.** Work of Separating the NBDs for the Six Simulations and the Resulting Angle between the Separated NBDs Calculated in the Protein Membrane Plane<sup>a</sup>

system	work (kJ/mol)	final inter-NBD angle (deg)
SMD-ADP1	1050.34	$2 \pm 2$
SMD-ADP2	1041.60	$28 \pm 2$
SMD-ADP-ML	685.75	$35 \pm 2$
SMD-APO1	629.35	$7 \pm 2$
SMD-APO2	780.86	$10 \pm 1$
SMD-APO-ML	572.60	$5 \pm 2$

<sup>a</sup>Angle uncertainty is the standard deviation of the last 2 ns of SMD simulation. See Table 1 for a description of each system.

Although we used a slow pulling rate of 0.1 nm/ns, we were unable to sample the opening of the TMD domain as observed in P-glycoprotein structures (pdb 3G5U<sup>42</sup>) or in both the open and closed inward-facing structure of MsbA<sup>19</sup> for any of the six simulations. In the lower extremities of the TMD a few contacts were broken during SMD, resulting in a semiopen state. In the crystal structure, TMDs make contacts with the NBDs through coupling with helices: the S108-N115  $\alpha$ -helix CH1 (CH3 on the second TMD) linking TMD helices H2 and H3 (H8-H9 on the second TMD) makes contacts with both NBDs and one ADP at the NBD's interface. The G209-F216  $\alpha$ -helix CH2 (CH4 on the second TMD) linking TMD helices H4 and H5 (H10-H11 on the second TMD) makes contact with the opposite NBD (see Figure 6). The open P-glycoprotein structure<sup>42</sup> features contacts between the CH1 and CH3 helices and their sequentially closest NBD domain which differs from our SMD results by a tilt of the NBDs bringing the C-terminal extremities closer while keeping the centers of mass of the two NBDs in place and opening the TMD core in a clothespin-like motion. In all SMD simulations, we observe a break of contact between the NBDs and the CH1 and CH3 helices, but not with the CH2 and CH4 helices. We also see that, in all cases, the ADP's phosphate groups stay in contact with the conserved Walker A motif G374-S381.<sup>18,43,44</sup>

Since the SMD simulations on wild-type SAV1866 structure did not generate separation events of the TMDs, we opted to extend the simulation time in which the protein's NBDs are separated.

**Constant-Restraint Molecular Dynamics.** Using constant-restraint molecular dynamics (CMD) and the result of three wild-type SMD simulations, we extended the simulation time of the semiopened states by 14 ns. We maintained the distance between the NBD centers of masses constant at 2.0 nm in order to let the protein react to the external force. On short time scales, the results showed little deformation of the protein, as shown in Figure 9.

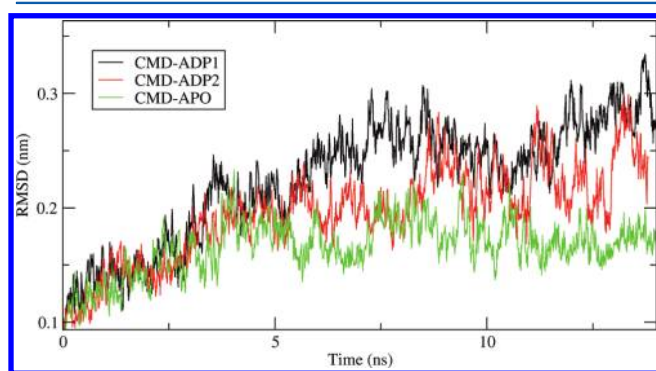


**Figure 9.** Evolution of the rmsd during constant-restraint MD simulation starting from the 20 ns time structure of SMD-ADP1, SMD-ADP2, and SMD-APO1 simulations.

To ensure that the time scale was sufficient for large-scale motion, we tested the reversibility of the conformational change imposed by SMD. From the CMD conformation obtained, the refolding MD simulations were launched by removing the restraints. Unrestrained MD simulations for the final structure of SMD-ADP1 (parallel separation) and SMD-APO1 (skewed separation of 7.5°) show a rapid refolding (25 ns) followed by little structure improvement in rmsd as shown in Figure 10.

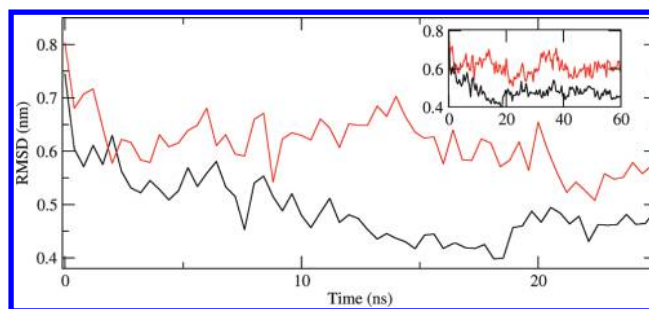


**Figure 10.** Rmsd evolution of the refolding simulation MD-ADP-RF (black) and MD-APO-RF (red) to the initial SMD conformations from SMD-ADP1 and SMD-APO1 respectively. Inset represents the whole 60 ns length of the refolding simulations.

In both cases, refolding was incomplete with a minimum rmsd of 0.40 nm in the ADP-bound simulation after 18 ns (MD-ADP-RF) and with a minimum rmsd of 0.51 nm after 23 ns for the APO simulation (MD-APO-RF) with initial unfolded rmsd were of 0.75 and 0.80 nm, respectively. While the presence of ADP may be driving a faster refolding process in comparison to the APO simulation, it may also be hindering it at the end when the ADPs' phosphates are still in contact with the Walker A motif<sup>43</sup> and the other atoms are no longer in the crystal structure orientation. Irrespective of the impact of the ADP, these observations show that large-scale motion is possible within our simulation time scale.

**Mutation Assay.** With the TMD stability being the limiting factor in observing the full opening of an ABC transporter, methods that target or destabilize the TMD may be needed. We attempted to destabilize the core interface of the TMD by the double H204A mutation. In Figure 7, His204 of helices H4 and H10 are highlighted in cyan and magenta, respectively, to illustrate the stability of these contacts after 2.0 nm of NBD separation. In the conventional MD simulations, His204 of H4 and H10 is in contact with its mirror image 96% of the simulation time, with Gln116 of H3 and H9 91% of the time, Gln208 of the opposite H10 and H4 52% of the time, as well as hydrophobic Val117 and Gly118 of H3 and H9 52% and 59% of the time, respectively. Its position at the core of the cytosolic extremity of the TMD indicates that it must be one of the first residues to break contact when the TMDs separate in the opening process. We designed the H204A mutant to evaluate the possibility of separating the TMD through SMD. Starting from the 100 ns conformation of the ADP-bound MD-ADP, His204 side-chain atoms were replaced by an alanine methyl group. The system was relaxed and two SMD following the same protocol were performed. The first, SMD-ADP-H204A1, is similar to the previous SMD-ADP1 simulation with respect to the TMD stability and NBD interdomain angle, converging to an angle of  $7 \pm 3^\circ$ . The second, SMD-ADP-H204A2, displays two new characteristics: (1) the c-terminal of one NBD stays in contact with its counterpart NBD throughout the simulation, effectively unfolding its secondary structure (see Figure 1 f); and (2) the gap left by the alanine mutation is not filled by neighboring amino acids like in the SMD-ADP-H204A1 run. Instead, a tunnel is left open, filled by roughly 8 water molecules.

## CONCLUSIONS

By studying a bacterial homologue of P-glycoprotein, a protein of vast interest in drug research, our goal was to elucidate some

elements of the conformational intermediates leading to the open and active form. SAV1866 is a very stable protein in MD simulation time scales. The conformational changes we observed in the membrane-inserted TMD region in both our ADP-bound and APO simulations were also found in APO simulation of Becker et al., but not in their ATP + Mg<sup>2+</sup> simulation.<sup>13</sup> SAV1866 was also crystallized with a homologue of ATP, namely AMP-PNP + Na<sup>+</sup> bound in its NBDs (pdb 2ONJ<sup>45</sup>). Although more negative than ATP + Mg<sup>2+</sup> (by one charge), it still holds the same structure as the ADP-bound case.<sup>18</sup> These conformational changes have not been previously reported,<sup>15,21</sup> and hence independent simulations and experiments are needed to examine if they have been overlooked in previous simulations or are a simulation artifact.

Stability of the NBD during steered deformation is affected by the bilayer and the ADP, as suggested by the work exerted by the harmonic potential to steer the protein to a semiopen state. The stability of the TMD remains unaffected in all cases. The extra work needed to separate the ADP-bound NBDs is in agreement with the targeted MD results performed on MsbA<sup>16</sup> which reported increased stability for their ATP + Mg<sup>2+</sup> simulations compared to the APO simulations. However, the separation pathways and the final states of the TMD were not influenced by the lipid bilayer or the ADP.

The fact that in all our ADP-bound simulations the ADP stayed in contact with the Walker A motif<sup>43</sup> throughout the 20 ns of SMD simulation is a clear indication that this motif may be the recruitment factor for ATP in an open conformation. The observed minimum angle peak of 10° between the NBDs during separation may indicate that a peeling separation may be energetically preferable, at least initially. A similar NBD angle was observed in the MD simulations of Jones et al.<sup>22</sup> when the NBDs were populated by only one ATP and where the distance in the APO half of the NBD pair grew more distant. This suggests a coordinated sequential hydrolysis of ATP.

Deformations of the NBD are reversible on a short time scale by removal of the restraints. The fast stabilization of these refolding simulations points to an unstable conformation forced by SMD. The observed stability suggests that the ATP hydrolysis energy exchange time scale between the ABC and TMD is beyond the scope of our MD simulations. Contrary to the simulations of Oliveira et al.<sup>21</sup> where a wide range of deformations including spontaneous separation of the TMDs in ATP-bound and ADP+IP-bound simulations were observed, the cytosolic side of our MD simulations was uneventful. When comparing our simulation protocol with that of Oliveira et al.,<sup>21</sup> none of their doubly protonated histidines that are singly protonated in our work are close to the cytosolic TMD regions shown to open and only the H534 might contribute to the stability of the NBDs. Our SMD assay on the H204A mutants demonstrated that a single-point mutation was not sufficient to destabilize the TMD interface and provoke an opening of the TMD.

Our present work was conducted using the hypothesis that the energy expenditure of ATP hydrolysis was the driving factor of the ABC and TMD separation, so our SMD protocol is akin to injecting energy close to the hydrolysis site. In light of our results, we must consider that either the opening is energy-driven on a much slower time scale that can be sampled through SMD or the process is initiated by the allosteric effect of the presence of the products of ATP hydrolysis in the binding cavity, as was suggested in a recent numerical simulation.<sup>21</sup>

## AUTHOR INFORMATION

### Corresponding Author

\*E-mail: normand.mousseau@umontreal.ca

### Notes

The authors declare no competing financial interest.

## ACKNOWLEDGMENTS

This work was supported by the Natural Sciences and Engineering Research Council of Canada (M.K., N.M.), the Academy of Finland (T.R., M.K.), Canada Research Foundation (N.M.), and the GALENOS program (J.F.S.P., A.B.). We are grateful to the Réseau québécois de calcul de haute performance (RQCHP), SharcNet (www.sharcnet.ca), and the Finnish IT Centre for Science for their generous allocations of computer time.

## REFERENCES

- (1) Chan, L. M. S.; Lowes, S.; Hirst, B. H. *Eur. J. Pharm. Sci.* **2004**, *21*, 25–51.
- (2) Hollenstein, K.; Dawson, R. J.; Locher, K. P. *Curr. Opin. Struct. Biol.* **2007**, *17*, 412–418.
- (3) Linton, K. J. *Physiology* **2007**, *22*, 122–130.
- (4) Rees, D. C.; Johnson, E.; Lewinson, O. *Nat. Rev. Mol. Cell Biol.* **2009**, *10*, 218–227.
- (5) Schinkel, A. H.; Jonker, J. W. *Adv. Drug Delivery Rev.* **2003**, *55*, 3–29.
- (6) Gottesman, M. M.; Ling, V. *FEBS Lett.* **2006**, *580*, 998–1009.
- (7) Pan, Y.; Stocks, B. B.; Brown, L.; Konermann, L. *Anal. Chem.* **2009**, *81*, 28–35.
- (8) Oloo, E. O.; Tieleman, D. P. *J. Biol. Chem.* **2004**, *279*, 45013–45019.
- (9) Oloo, E. O.; Kandt, C. K.; Megan, L. O.; Mara, M. L.; Tieleman, D. P. *Biochem. Cell Biol.* **2006**, *84*, 900–911.
- (10) Oloo, E. O. *J. Biol. Chem.* **2006**, *281*, 28397–28407.
- (11) Ivetac, A.; Campbell, J. D.; Sansom, M. S. P. *Biochemistry* **2007**, *46*, 2767–2778.
- (12) Sonne, J.; Kandt, C.; Peters, G. H.; Hansen, F. Y.; Jensen, M. O.; Tieleman, D. P. *Biophys. J.* **2007**, *92*, 2727–2734.
- (13) Becker, J.-P.; Van Bambeke, F.; Tulkens, P. M.; Prevost, M. J. *Phys. Chem. B* **2010**, *114*, 15948–15957.
- (14) Kandt, C.; Tieleman, D. P. *Proteins* **2010**, *78*, 738–753.
- (15) Aittoniemi, J.; de Wet, H.; Ashcroft, F. M.; Sansom, M. S. P. *PLoS Comput. Biol.* **2010**, *6*, e1000762.
- (16) Weng, J.-W.; Fan, K.-N.; Wang, W.-N. *J. Biol. Chem.* **2010**, *285*, 3053–3063.
- (17) Aller, S. G.; Yu, J.; Ward, A.; Weng, Y.; Chittaboina, S.; Zhuo, R.; Harrell, P. M.; Trinh, Y. T.; Zhang, Q.; Urbatsch, I. L.; Chang, G. *Science* **2009**, *323*, 1718–1722.
- (18) Dawson, R. J. P.; Locher, K. P. *Nature* **2006**, *443*, 180–185.
- (19) Ward, A.; Reyes, C. L.; Yu, J.; Roth, C. B.; Chang, G. *Proc. Natl. Acad. Sci. U.S.A.* **2007**, *104*, 19005–10.
- (20) Velamakanni, S.; Yao, Y.; Gutmann, D. A. P.; van Veen, H. W. *Biochemistry* **2008**, *47*, 9300–9308.
- (21) Sofia Oliveira, A.; Baptista, A. M.; Soares, C. M. *Proteins* **2011**, *79*, 1977–1990.
- (22) Jones, P. M.; George, A. M. *Biophys. J.* **2011**, *100*, 3025–3034.
- (23) Sankaran, B.; Bhagat, S.; Senior, A. E. *Biochemistry* **1997**, *36*, 6847–6853.
- (24) Zaitseva, J.; Oswald, C.; Jumpertz, T.; Jenewein, S.; Wiedenmann, A.; Holland, I. B.; Schmitt, L. *EMBO J.* **2006**, *25*, 3432–3443.
- (25) Zolnerciks, J. K.; Wooding, C.; Linton, K. J. *FASEB J.* **2007**, *21*, 3937–3948.
- (26) Hess, B.; Kutzner, C.; van der Spoel, D.; Lindahl, E. *J. Chem. Theory Comput.* **2008**, *4*, 435–447.
- (27) Jorgensen, W.; Tirado-Rives, J. *J. Am. Chem. Soc.* **1988**, *110*, 1657–1666.

- (28) Darden, T.; York, D.; Pedersen, L. J. *Chem. Phys.* **1993**, *98*, 10089–10092.
- (29) Karttunen, M.; Rottler, J.; Vattulainen, I.; Sagui, C. *Curr. Top. Membr.* **2008**, *60*, 49–89.
- (30) Wong-Ekkabut, J.; Miettinen, M. S.; Dias, C.; Karttunen, M. *Nat. Nanotechnol.* **2010**, *5*, 555–557.
- (31) Patra, M.; Karttunen, M.; Hyvönen, M.; Falck, E.; Lindqvist, P.; Vattulainen, I. *Biophys. J.* **2003**, *84*, 3636–3645.
- (32) Patra, M.; Karttunen, M.; Hyvönen, M. T.; Falck, E.; Vattulainen, I. *J. Phys. Chem. B* **2004**, *108*, 4485–4494.
- (33) Róg, T.; Martinez-Seara, H.; Munck, N.; Oresic, M.; Vattulainen, M. K. I. *J. Phys. Chem. B* **2009**, *113*, 3413–3422.
- (34) Stepniewski, M.; Bunker, A.; Pasenkiewicz-Gierula, M.; Karttunen, M.; Rog, T. *J. Phys. Chem. B* **2010**, *114*, 11784–11792.
- (35) Dror, R. O.; Arlow, D. H.; Borhani, D. W.; Jensen, M.; Piana, S.; Shaw, D. E. *Proc. Natl. Acad. Sci. U.S.A.* **2009**, *106*, 4689–4694.
- (36) Jorgensen, W. L.; Chandrasekhar, J.; Madura, J. D.; Impey, R. W.; Klein, M. L. *J. Chem. Phys.* **1983**, *79*, 926–935.
- (37) Hess, B.; Bekker, H.; Berendsen, H. J. C.; Fraaije, J. G. E. M. *J. Comput. Chem.* **1997**, *18*, 1463–1472.
- (38) Berendsen, H.; Postma, J.; Vangunsteren, W.; Dinola, A.; Haak, J. J. *J. Chem. Phys.* **1984**, *81*, 3684–3690.
- (39) Nosé, S. *Mol. Phys.* **1984**, *52*, 255–268.
- (40) Hoover, W. G. *Phys. Rev. A* **1985**, *31*, 1695–1697.
- (41) Parrinello, M.; Rahman, A. *J. Appl. Phys.* **1981**, *52*, 7182–7190.
- (42) Aller, S. G.; Yu, J.; Ward, A.; Weng, Y.; Chittaboina, S.; Zhuo, R.; Harrell, P. M.; Trinh, Y. T.; Zheng, Q.; Urbatsch, I. L.; Chang, G. *Science* **2009**, *323*, 1718–1722.
- (43) Schneider, E.; Hunke, S. *FEMS Microbiol. Rev.* **1998**, *22*, 1–20.
- (44) Linton, K.; Higgins, C. *Pflugers. Arch.* **2007**, *453*, 555–567.
- (45) Dawson, R. J.; Locher, K. P. *FEBS Lett.* **2007**, *581*, 935–938.